RSC Advances

PAPER

View Article Online
View Journal | View Issue

Cite this: *RSC Adv.*, 2015, **5**, 87496

Electronic structure and optical properties of $Zn(OH)_2$: LDA+*U* calculations and intense yellow luminescence†

Mingsong Wang,*[a] Lingxia Jiang,[a] Eui Jung Kim*[b] and Sung Hong Hahn[c]

Received 23rd August 2015
Accepted 8th October 2015

DOI: 10.1039/c5ra17024a

www.rsc.org/advances

The electronic structure of $Zn(OH)_2$ has been studied by first-principles calculations using the local density approximation + Hubbard *U* (LDA+*U*) scheme. Based on the LDA+*U* calculations of ZnO and $Zn(OH)_2$, a principle for the correct assignment of the *U* values has been established. The assigned *U* values should assure an appropriate overlap of the Zn 3d and O 2p states. Both theoretical calculations and experimental investigations have determined an energy band gap of 5.65 eV for $Zn(OH)_2$. We also report abnormal yellow luminescence of $Zn(OH)_2$ resembling that of ZnO. Characterizations of cathodoluminescence, UV-Vis absorption and X-ray photoelectron spectroscopy reveal that ZnO of several atomic layers in thickness covers the surface of $Zn(OH)_2$, which gives rise to the intense yellow luminescence observed for $Zn(OH)_2$.

1. Introduction

Zinc hydroxide ($Zn(OH)_2$) is an amphoteric compound, which normally crystallizes in wülfingite ε-$Zn(OH)_2$ with orthorhombic structure (space group $P2_12_12_1$) under ambient conditions.[1] This material readily dehydrates in air or under hydro(solvo)thermal conditions at elevated temperatures and transforms into ZnO.[2–5] Recent reports show that ε-$Zn(OH)_2$ could be an intermediate during the growth of ZnO in alkaline solution.[6–8] Several mechanisms, such as the dissolution of $Zn(OH)_2$ and the reprecipitation of ZnO, *in situ* crystallization, and solid–solid topotactic transition by lattice dehydration, have been proposed for the phase transformation from $Zn(OH)_2$ to ZnO in solution.[9–11] The topotactic transition from $Zn(OH)_2$ to ZnO indicates that the two materials are structurally correlated. Although ZnO is intensively studied as a wide band gap (3.37 eV) semiconductor,[12] yet very little is known about the electronic structure and optical properties of $Zn(OH)_2$.

During the past several decades the first-principles density-functional theory (DFT) based on the local density approximation (LDA) and the generalized gradient approximation (GGA) has been employed to investigate the electronic structure of wide band gap transition metal oxides.[13–17] An extension of the LDA method, *i.e.*, the LDA+*U* method, where the Hubbard parameter, *U*, is an on-site Coulomb repulsion parameter that incorporates part of the electron correlation absent in LDA, can reproduce the electronic energy bands accurately.[18–20] However, the *U* parameters for the d electrons (U_d) of transition metal and the p electrons (U_p) of oxygen are mostly empirically assigned.[19–21] Thus, it is necessary to examine the predictive ability of the LDA+*U* method by applying the same *U* parameters to calculate the electronic structures of structurally different compounds that consist of the same transition metal, *e.g.*, ZnO and $Zn(OH)_2$.

In this work, combined computational and experimental investigations on the electronic structure and optical properties of $Zn(OH)_2$ have been conducted. LDA+*U* calculations of the electronic structure of ZnO and $Zn(OH)_2$ have been systematically performed based on the identical *U* values. The energy band gap of $Zn(OH)_2$ predicted by the LDA+*U* calculation is in excellent agreement with the experimental results of 5.65 eV. Prepared by a simple coprecipitation method, $Zn(OH)_2$ is observed to emit intense yellow luminescence resembling that of ZnO under ultraviolet (UV) light excitation. A detailed discussion on the origin of the abnormal yellow luminescence from $Zn(OH)_2$ has been presented.

2. Methodology

2.1. Computational approach

The DFT calculations were carried out with the GGA method using the Perdew–Burke–Ernzerhof (PBE) exchange correlation potential implemented in the CASTEP code.[22] The

[a]School of Materials Science and Engineering, Jiangsu University, Zhenjiang 212013, China. E-mail: wangms@mail.ujs.edu.cn

[b]Department of Chemical Engineering, University of Ulsan, Ulsan 680-749, South Korea. E-mail: ejkim@ulsan.ac.kr

[c]Department of Physics and Energy Harvest-Storage Research Center, University of Ulsan, Ulsan 680-749, South Korea

† Electronic supplementary information (ESI) available: Calculated lattice constants, atomic and bond populations, energy band gap and density of states of ZnO and $Zn(OH)_2$. See DOI: 10.1039/c5ra17024a

ion–electron interaction was modeled by the ultrasoft pseudopotential in the Vanderbilt form with valence electron configurations of $4s^2 3d^{10}$ for Zn, $2s^2 2p^4$ for O, and $1s^1$ for H. The electron wave functions were expanded through a plane wave basis set and the cutoff energy was selected as 340 eV. For *k*-point sampling, Monkhorst–Pack meshes of $3 \times 3 \times 2$ and $3 \times 3 \times 4$ yielding grid spacing less than 0.05 $Å^{-1}$ in the first Brillouin zone were employed for the $3 \times 3 \times 2$ supercell of ZnO and $2 \times 2 \times 1$ supercell of $Zn(OH)_2$, respectively. The convergence threshold for self-consistent iteration was set at 5×10^{-6} eV per atom, and the lattice constants and all atomic positions for each supercell were fully relaxed until the maximal force on each atom was less than 0.01 eV $Å^{-1}$, the internal stress was below 0.02 GPa, and the displacement of each atom was below 5×10^{-4} Å. The LDA+*U* calculations were then performed after the geometry optimization of ZnO and $Zn(OH)_2$. To reproduce the electronic band gap (E_g) of ZnO consistent with its experimental value, both U_d for Zn 3d and U_p for O 2p were considered in the calculations. For example, U_d was varied at fixed U_p until an E_g of 3.37 eV was obtained for bulk ZnO (Fig. S1†). In this way, five groups of (U_p, U_d) values were determined, which were further employed for the calculation of the electronic structure of $Zn(OH)_2$.

2.2. Experimental details

$Zn(OH)_2$ was prepared by a coprecipitation method. Typically, 6.64 g $Zn(NO_3)_2 \cdot 6H_2O$ and 7.68 g NaOH were dissolved in 120 and 80 mL deionized water, respectively. The two solutions were then mixed at 0 °C under constant stirring. The solution became turbid in 5 min, indicating the precipitation of $Zn(OH)_2$ crystals. After a 10 min reaction, a white precipitate was harvested by centrifugation and subsequently washed with deionized water for several times, and finally dried at 60 °C overnight. Structural characterization of the precipitate was carried out using an X-ray diffractometer (XRD, Bruker Axs D8 Advance) with Cu Kα radiation. Raman spectra were obtained at room temperature from a laser Raman spectrometer (SPEX 1403) with a He–Ne laser at an excitation wavelength of 632.8 nm. The thermogravimetric (TG) analysis was conducted on a TA Q50 instrument (Universal Analysis 2000) under N_2/air flow of 60/40 mL min^{-1} at a heating rate of 10 °C min^{-1}. The optical absorbance of the precipitates was measured by using a double beam UV-Vis spectrophotometer (Shimadzu UV2550). Photoluminescence (PL) spectra were recorded at room temperature by exciting the samples with a 325 nm He–Cd laser at an output power of 30 mW (IK3301R-G) as well as a 150 W Xe lamp (Horiba Jobin Yvon fluorometer) at an excitation wavelength of 353 nm. Room temperature cathodoluminescence (CL) measurements were carried out *in situ* in a scanning electron microscope (SEM, Sirion200) integrated with a Gatan Mono CL system. Chemical compositions were analyzed by using an X-ray photoelectron spectroscope (XPS, Thermo ESCALAB 250). A monochromated Al Kα source (1483.6 eV) was used with the analyzer mode set at constant pass energy of 20 eV. All the peak energies in the spectra were referenced with respect to the C 1s peak (284.8 eV) arising from adventitious carbons.

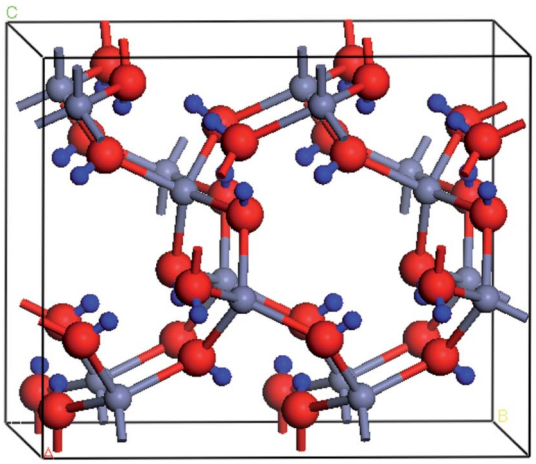

Fig. 1 Structure model of a $2 \times 2 \times 1$ ε-$Zn(OH)_2$ supercell. Red, gray, and blue spheres represent O, Zn, and H atoms, respectively.

3. Results and discussion

3.1. Electronic structure of $Zn(OH)_2$ by LDA+*U* calculations

Fig. 1 presents the structure model of a $2 \times 2 \times 1$ ε-$Zn(OH)_2$ supercell employed in the calculation. As illustrated in Fig. 1, each zinc ion is surrounded by four hydroxyl ions, while each hydroxyl ion is coordinated with two zinc ions. Geometry optimization of ZnO and $Zn(OH)_2$ is performed prior to the LDA+*U* calculations. The optimized cell parameters are shown in Table S1.† The deviation in cell volume between the calculated and experimental values is less than 1%, indicating that our calculations are reliable. Mulliken population analysis shows that Zn becomes more positively charged, while O sees a slight increase in its negative charge in $Zn(OH)_2$ when compared with their charges in ZnO (Table S2†). This means that Zn contributes more electrons to O in $Zn(OH)_2$, indicating an increased Coulomb attraction between Zn and O. The deceased O–Zn bond populations in $Zn(OH)_2$ further confirm this fact, although some of the O–Zn bond lengths are larger than those in ZnO (Table S3†). Note also that in $Zn(OH)_2$ the O–H bonds between adjacent OH ions are highly ionized (bond population 0.09), while those within the OH ions are predominantly covalent (bond population 0.61) (Table S3†).

To systematically investigate the LDA+*U* approach, five groups of (U_p, U_d) parameters, *i.e.*, (6.50, 13.60), (7.00, 9.80), (7.50, 7.32), (8.00, 5.57) and (8.50, 4.26), are determined to reproduce an E_g of 3.37 eV for ZnO. Although these *U* parameters can reproduce the correct E_g for ZnO (the DOSs in the VBM and conduction band (CB) are nearly the same), the DOSs in the lower valance band vary with the *U* values (Fig. 2). More specifically, the states in the range of −16 to −14 eV and −10 to −3 eV are shifted to the higher energy side with increasing U_p or decreasing U_d values. To understand these changes, the DOSs for ZnO are calculated at fixed U_p (U_d). As shown in Fig. S2a,† the DOSs (except those in the VBM) are uniformly shifted up with increasing U_p. However, a shift toward lower energy in the range of −9 to −3 eV and a shift up in the CB are observed at higher U_d

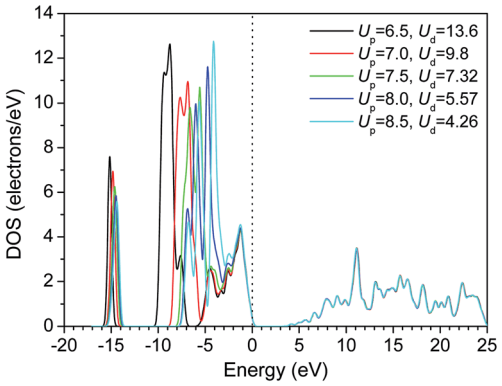

Fig. 2 DOSs for ZnO calculated with LDA+U using various U parameters.

(Fig. S2b†). Thus, the variation of the DOSs in the lower valance band in Fig. 2 can be understood as follows: the shift of O 2s states from −16 to −14 eV is mainly ascribed to the increased U_p values, while the dual effect of increasing U_p and decreasing U_d results in a shift up of the hybridization states of Zn 3d and O 2p in the range of −10 to −3 eV. On the other hand, the opposite effect of increasing U_p and decreasing U_d makes the states in the CB unchanged. As a consequence, the five groups of (U_p, U_d) parameters result in the same E_g (3.37 eV) for ZnO.

It is well known that the DFT calculations based on LDA and GGA underestimate the band gap of many transition metal oxides, due to the artificially large p–d coupling pushing up the valence band maximum (VBM).[23] Here, the dependence of the p–d coupling on the U parameters is investigated. The hybridization between Zn 3d and O 2p as a function of the U values is illustrated in terms of the electron density contour maps and the DOSs. As is easily seen in Fig. 3a–e, the electron density of Zn 3d decreases with decreasing U_d, while that of O 2p increases with increasing U_p. Furthermore, the p–d coupling is enhanced at higher U_p and lower U_d values as the increased overlap of the two states can be identified in the electron density contour maps as well as the DOSs (Fig. 3). Thus, it seems that there exists optimal U values correctly describing the p–d coupling. Considering the atomic populations for O 2p (5.11e) and Zn 3d (9.98e) (Table S2†), the electron density of Zn 3d should be nearly twice as large as that of O 2p. Therefore, U_p = 7.0 and U_d = 9.8 should provide more accurate description of the electronic states of O 2p and Zn 3d, respectively, as judged from their relative electron density in the electron density contour maps in Fig. 3b.

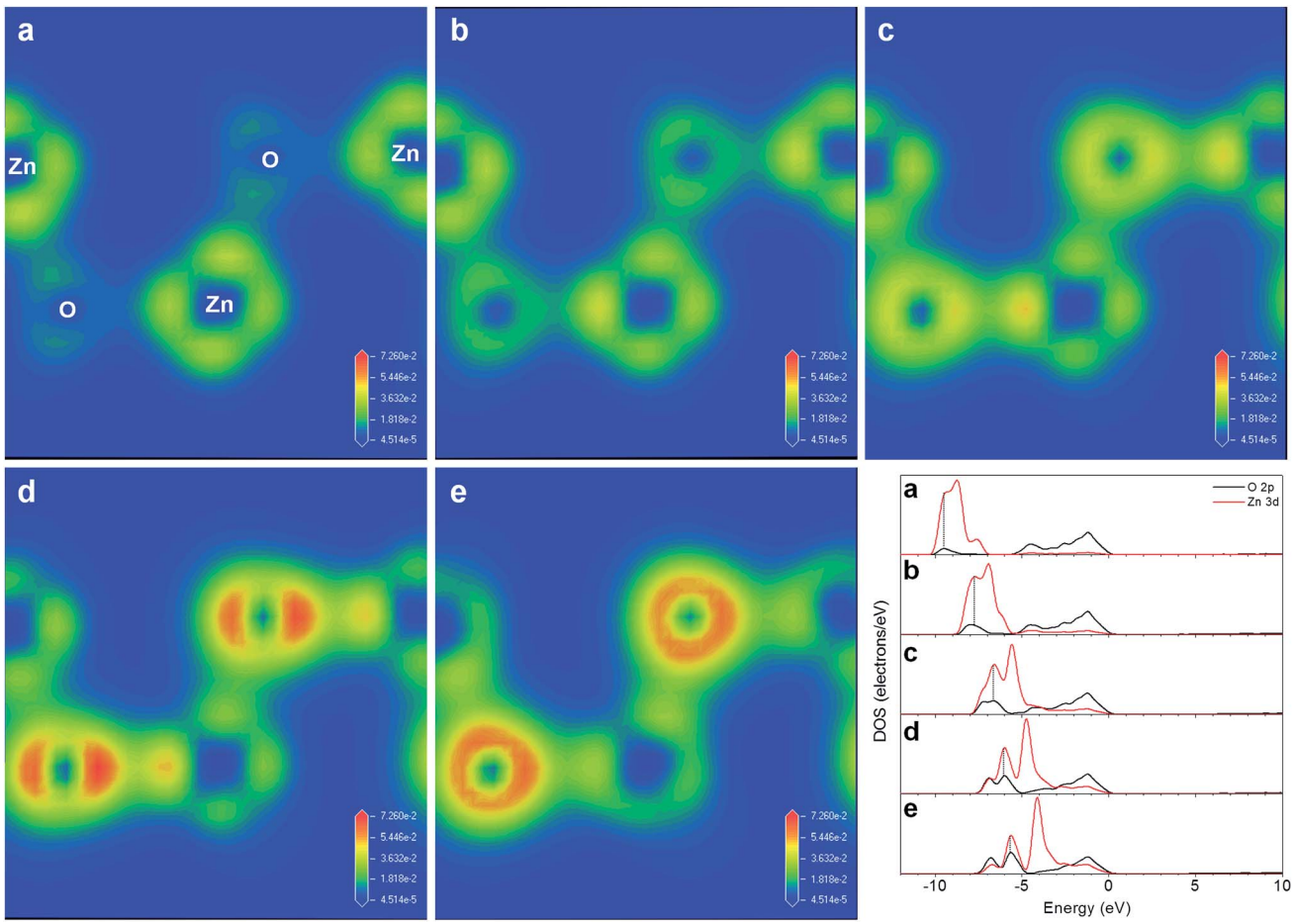

Fig. 3 Electron density contour maps and the corresponding DOSs showing the hybridization of Zn 3d and O 2p for ZnO calculated with LDA+U using various U parameters: (a) U_p = 6.5, U_d = 13.6; (b) U_p = 7.0, U_d = 9.8; (c) U_p = 7.5, U_d = 7.32; (d) U_p = 8.0, U_d = 5.57; (e) U_p = 8.5, U_d = 4.26.

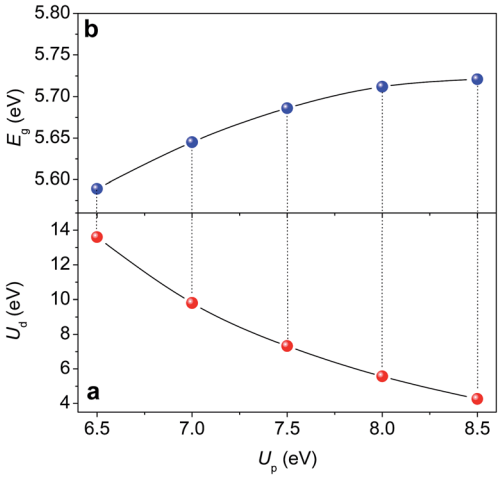

Fig. 4 Determined $U_d + U_p$ values for the reproduction of E_g of 3.37 eV for ZnO (a) and their employment for the calculation of E_g for $Zn(OH)_2$ (b).

Now we apply the five groups of (U_p, U_d) parameters to predict the E_g of $Zn(OH)_2$. The calculated E_g of $Zn(OH)_2$ as a function of (U_p, U_d) values is plotted in Fig. 4. The E_g of $Zn(OH)_2$ is found to increase from 5.589 to 5.721 eV with increasing (decreasing) U_p (U_d). This expanding in E_g is ascribed to a slight shift of the CB as observed in the calculated DOSs (Fig. S3†). The other variations in the DOSs for $Zn(OH)_2$ with different U values are similar to those for ZnO (Fig. 2 and S3†). As discussed above, considering the atomic populations of O 2p (5.17e) and Zn 3d (9.99e) for $Zn(OH)_2$ (Table S2†), $U_p = 7.0$ and $U_d = 9.8$ should reproduce a more accurate E_g (5.645 eV) because of their better description of the electronic states. As is shown below, the calculated E_g is in excellent agreement with the experimental one of 5.65 eV. Thus, a principle can be set to the assignment of the U parameters in the LDA+U calculations. Beyond the empirical adjustment of the U values to achieve a correct E_g, which is currently employed in most LDA+U calculations,[19–21] the employed U_p (U_d) values should keep the relative electron density of O 2p and Zn 3d consistent with their atomic populations so as to achieve an appropriate overlap of the two states.

Fig. 5 presents the calculated band structure and DOSs of $Zn(OH)_2$ with $U_p = 7.0$ and $U_d = 9.8$. A direct E_g of 5.645 eV is obtained at the G point (Fig. 5a). It is seen from the partial DOSs shown in Fig. 5b that the Zn sp^3 hybridization states contribute dominantly to the CB, while the VBM mainly consists of O 2p states. The hybridization states of Zn 3d and O 2p as well as H 1s and O 2s are responsible for the lower VB ranging from −7.3 to −5.5 eV and −15.5 to −14 eV, respectively.

3.2. Yellow luminescence from $Zn(OH)_2$

Fig. 6 shows the typical XRD pattern of the as-prepared $Zn(OH)_2$. All diffraction peaks are consistent with those in the simulated pattern, suggesting that the as-prepared $Zn(OH)_2$ possesses a wülfingite structure. Note that no impurity phase such as ZnO can be identified in Fig. 6. Raman measurement is further carried out to investigate the phase purity of the as-prepared

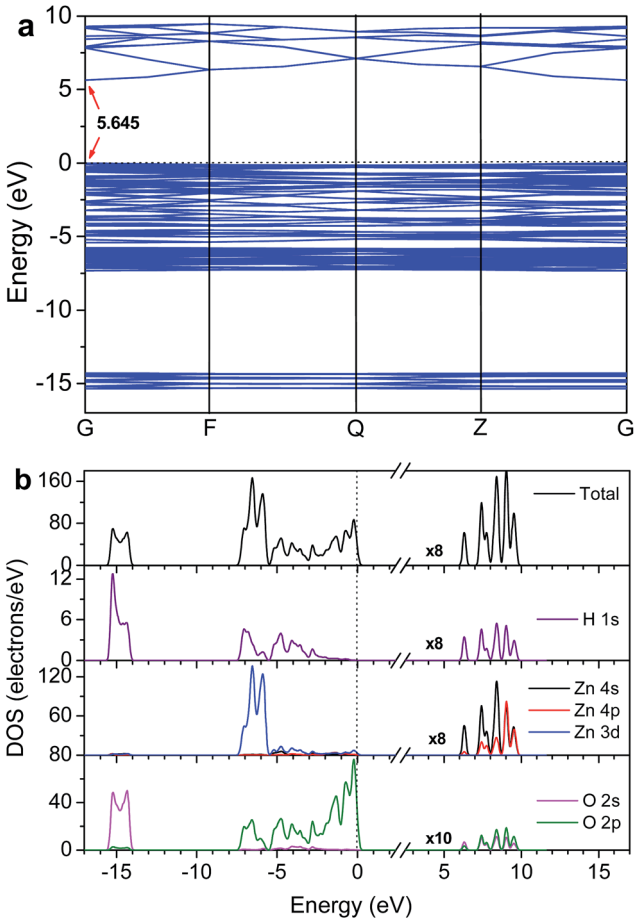

Fig. 5 Band structure (a) and DOSs (b) of $Zn(OH)_2$ calculated with LDA+U ($U_p = 7.0$, $U_d = 9.8$).

$Zn(OH)_2$. In Fig. 7 all Raman bands are ascribed to the characteristic modes of ε-$Zn(OH)_2$.[24] Two strong Raman bands at 367 and 381 cm^{-1} are attributed to the symmetric Zn–O stretching modes of the ZnO_4 tetrahedron in $Zn(OH)_2$, while two weak bands at 479 and 720 cm^{-1} are assigned to the translational modes and the OH librations, respectively.[24] As shown in Fig. 7,

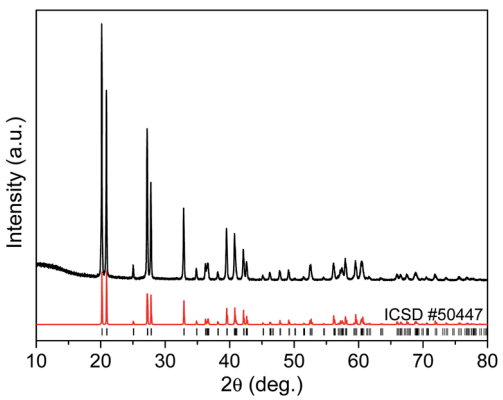

Fig. 6 XRD pattern of the as-prepared $Zn(OH)_2$. The simulated XRD pattern according to ICSD #50447 for ε-$Zn(OH)_2$ is included for comparison.

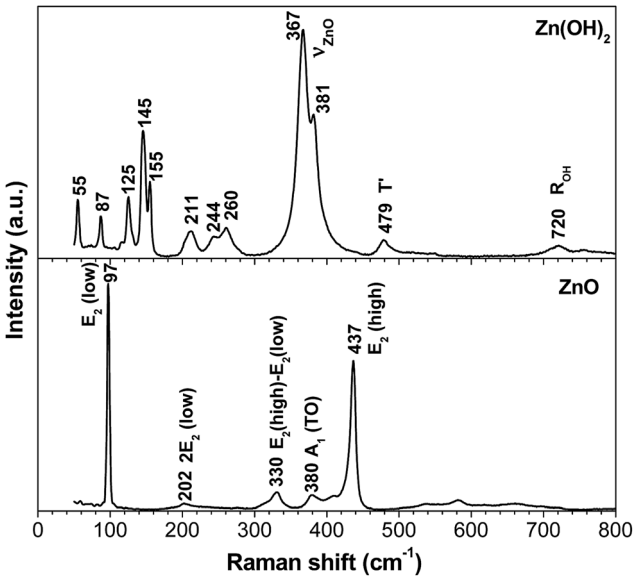

Fig. 7 Raman spectra of the as-prepared $Zn(OH)_2$ and ZnO. ZnO is prepared by annealing $Zn(OH)_2$ in air at 600 °C for 1 h.

no characteristic modes of ZnO could be found in the Raman spectra of $Zn(OH)_2$. Thus, both XRD and Raman measurements confirm a pure phase of the as-prepared $Zn(OH)_2$.

TG analysis of the as-prepared $Zn(OH)_2$ is plotted in Fig. 8. A steep weight loss of 16.5% is observed from 119 to 153 °C, which is followed by a slow weight loss of 1.6% until 600 °C. The former is obviously due to the decomposition of $Zn(OH)_2$. However, the weight loss of 16.5% is smaller than the theoretical values of 18.1% predicted by the chemical formula. A total weight loss of 18.1% is reached at 600 °C, indicating that the thermal decomposition of $Zn(OH)_2$ is not completed until 600 °C.[25] Unfortunately, the exact mechanism of the slow decomposition process at temperatures higher than 153 °C is still not clear at the present time.

The above characterizations indicate that a pure $Zn(OH)_2$ is synthesized. Below we will discuss its optical properties. Fig. 9 depicts the PL spectra of $Zn(OH)_2$. The PL spectra of ZnO obtained by thermal decomposition of $Zn(OH)_2$ is also included for comparison. As seen in Fig. 9, a weak UV emission at 387 nm

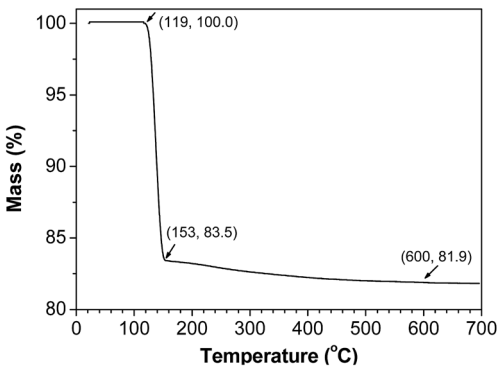

Fig. 8 TG curve of the as-prepared $Zn(OH)_2$.

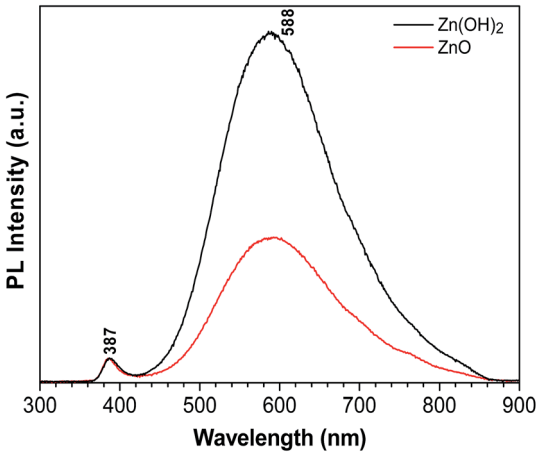

Fig. 9 PL spectra of the as-prepared $Zn(OH)_2$ and ZnO. ZnO is prepared by annealing $Zn(OH)_2$ in air at 600 °C for 1 h. A 325 nm He–Cd laser is used as the excitation source.

and an intense yellow luminescence centered at 588 nm are generated from $Zn(OH)_2$ under the excitation of a 325 nm He–Cd laser. This yellow luminescence is strong enough to be visible to the naked eyes. The two emission bands of $Zn(OH)_2$ are nearly identical to those of ZnO, except that the yellow luminescence is less intense for ZnO. The UV band is known as the near-band-edge emission of ZnO, while the yellow luminescence is attributed to the deep-level emission from oxygen interstitials (O_i), where the recombination of a delocalized electron close to the conduction band with a deeply trapped hole in the O_i centers gives out yellow light.[26,27] We note that yellow luminescence is frequently observed from ZnO grown in an aqueous solution,[28] implying an excess of oxygen in the solution-grown ZnO.[29] Thus, it is demonstrated that $Zn(OH)_2$ amazingly replicates the PL properties of ZnO. To corroborate this observation, the PL spectra of $Zn(OH)_2$ excited by an Xe lamp are also taken. As illustrated in Fig. 10, an intense yellow luminescence is generated with the band peaked at 570 nm.

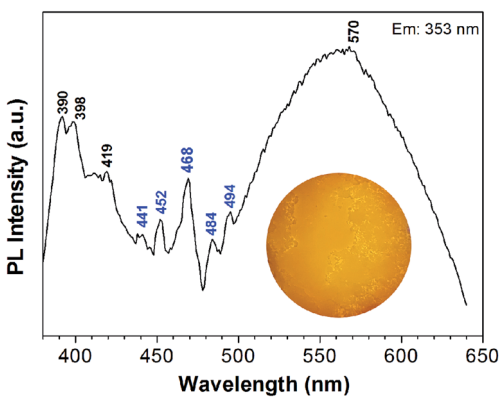

Fig. 10 PL spectra of the as-prepared $Zn(OH)_2$ under the excitation of a Xe lamp. The excitation wavelength is 353 nm. The inset shows the photograph of yellow luminescence from $Zn(OH)_2$ under UV irradiation.

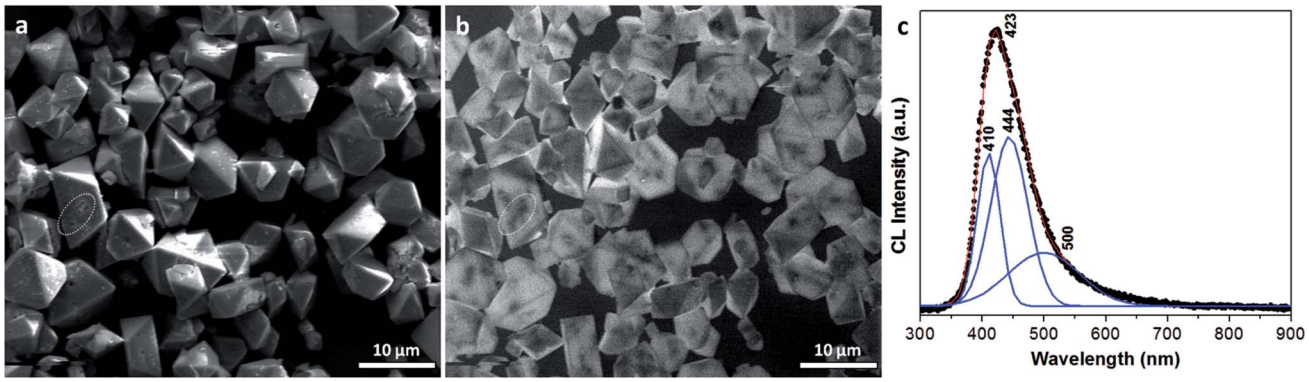

Fig. 11 SEM image (a) and the corresponding CL image (b) and CL spectra (c) of the as-prepared $Zn(OH)_2$. The enclosed area in (a) and (b) indicates no CL is generated from the defective holes.

Several sharp peaks ranging from 441 to 494 nm also appear, which should arise from the Xe lamp[30,31] rather than the emissions of ZnO.[29,32–35] A UV peak at 390 nm may be due to the near-band-edge emission of ZnO. Again, a typical PL of ZnO is observed for $Zn(OH)_2$. The inset photograph of Fig. 10 undoubtedly confirms the yellow luminescence from $Zn(OH)_2$.

CL measurement is further performed to study the origin of the luminescence from $Zn(OH)_2$. In Fig. 11b, the CL is observed to distribute uniformly across the $Zn(OH)_2$ crystals. A close look at Fig. 11a and b reveals that no CL is generated from the defective holes on the surface of the $Zn(OH)_2$ microcrystals. This implies that the CL is from the surface of $Zn(OH)_2$. The CL spectra shown in Fig. 11c, however, are quite different from the PL data. A broad violet emission centered at 423 nm is observed, which can be resolved into three bands at 410, 444 and 500 nm. Violet emission has been occasionally observed from ZnO.[36] The visible emission from ZnO may shift with the excitation wavelength.[37] Provided that the CL from $Zn(OH)_2$ is also related to ZnO, the difference between the CL and PL spectra might be due to the different excitation source employed.

The optical properties of the as-prepared $Zn(OH)_2$ are investigated in terms of UV-Vis absorption. Interestingly, two sharp absorption edges with peaks located at 219.6 and 368.6 nm are observed in Fig. 12, which are assigned to the band edge absorption of $Zn(OH)_2$ and ZnO, respectively. The corresponding E_g determined by the optical absorption is 5.65 and 3.37 eV for $Zn(OH)_2$ and ZnO, respectively. Note that the experimentally determined E_g for $Zn(OH)_2$ and ZnO agrees quite well with the theoretically calculated values. The double absorption edges were previously observed for the layered $Zn(OH)_2$.[38] The authors did observe a ZnO-induced absorption edge at 370 nm, but they did not realize that the absorption edge at around 220 nm is due to $Zn(OH)_2$.[38] The absorption spectrum in Fig. 12 provides strong evidence that the structurally confirmed "pure" $Zn(OH)_2$ does contain ZnO. The possible explanations are as follows: the detection depth for characterizations such as XRD and Raman is rather deep such that they can only obtain the bulk phase information. Instead, optical characterizations such as PL, CL and UV-Vis absorption is very sensitive to the surface so that a lot of surface information can be obtained. As revealed by the CL image in Fig. 11b, the CL is from the surface of $Zn(OH)_2$. Thus, we can reasonably assume that a thin layer of ZnO is formed on the surface of $Zn(OH)_2$.

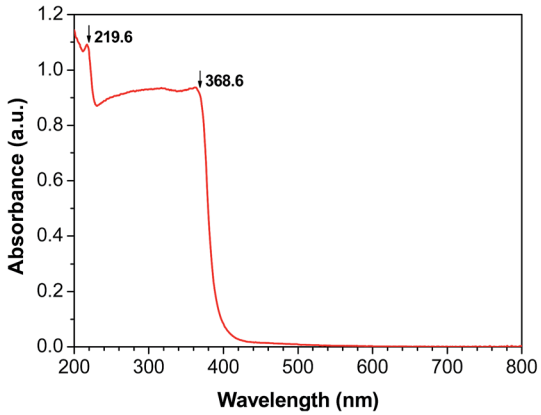

Fig. 12 UV-Vis absorption spectrum of the as-prepared $Zn(OH)_2$.

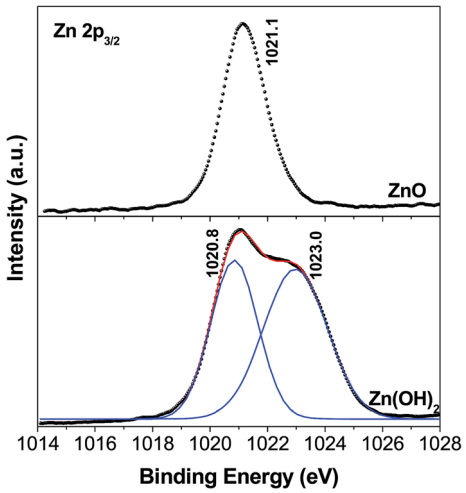

Fig. 13 Zn $2p_{3/2}$ XPS spectra of the as-prepared $Zn(OH)_2$ and ZnO. ZnO is prepared by annealing $Zn(OH)_2$ in air at 600 °C for 1 h.

To confirm the existence of ZnO outer layer, the surface chemistry of $Zn(OH)_2$ is studied by XPS. Fig. 13 shows the XPS spectra of Zn $2p_{3/2}$ core level for the as-prepared $Zn(OH)_2$ and ZnO. The Zn $2p_{3/2}$ core level obtained for $Zn(OH)_2$ is quite broad, which can be deconvoluted into two components located at 1020.8 and 1023.0 eV. The high-energy peak at 1023.0 eV is ascribed to the Zn^{2+} in the hydroxide.[39,40] The low-energy peak at 1020.8 eV is consistent with the 1021.1 eV for ZnO, thus it should be associated with the Zn^{2+} in the wurtzite ZnO.[41,42] The sampling depth for Zn $2p_{3/2}$ is estimated to be about 3.5 nm.[43] Therefore, the thickness of ZnO layer on $Zn(OH)_2$ is determined to be *ca.* 1.5 nm based on the two decomposed band areas of the Zn $2p_{3/2}$ spectra for $Zn(OH)_2$. Being covered with several atomic layers of ZnO, $Zn(OH)_2$ works efficiently as ZnO emitting intense yellow luminescence (Fig. 9 and 10). Earlier works showed that the green emission of ZnO is strongly correlated with surface,[43,44] and so is the yellow luminescence from $Zn(OH)_2$. Our findings herein indicate a possible application of $Zn(OH)_2$ as a phosphor, and the characteristic surface emission may be exploited to design new phosphors by simply coating a thin layer of luminescent material.

However, it is not clear how ZnO is formed on the surface of $Zn(OH)_2$. Our previous work showed both ZnO and $Zn(OH)_2$ can be grown from alkaline solution at room temperature by controlling the pH value, but the two materials have quite different morphologies.[6] Since the preparation conditions are far below the decomposition temperature ($\geq$119 °C, Fig. 8) of $Zn(OH)_2$, the formation of ZnO by thermal decomposition can be excluded. We have proposed a mechanism of lattice dehydration between adjacent hydroxyl ions to explain the solid phase transition from $Zn(OH)_2$ to ZnO.[11] The surface of $Zn(OH)_2$ contains many dangling OH^- ions, which are energetically higher than those in the bulk due to a lack of full coordination of the ions. These OH^- ions, therefore, might dehydrate between adjacent ones to increase coordination and form ZnO.

4. Conclusions

We have probed into the electronic structure and optical properties of $Zn(OH)_2$ by means of both theoretical calculations and experimental investigations. LDA+U calculations have been explored with systematically adjusted U_p (U_d) values for ZnO and $Zn(OH)_2$. A principle is established for the correct description the electronic states by LDA+U, *i.e.*, the U parameters are tuned so that an appropriate overlap of the O 2p and Zn 3d orbitals is reached. With this principle, U_p and U_d are determined as 7.0 and 9.8, respectively. Our theoretical simulation accurately predicts an experimentally consistent E_g of 3.370 and 5.645 eV for ZnO and $Zn(OH)_2$, respectively. Interestingly, the yellow luminescence of ZnO is observed for $Zn(OH)_2$. Although the XRD and Raman spectra do not provide any information about ZnO, the UV-Vis spectra reveal the coexistence of ZnO with $Zn(OH)_2$. CL and XPS analyses probe a thin layer of ZnO covering the surface of $Zn(OH)_2$, which is responsible for the intense yellow luminescence generated.

Acknowledgements

This work was supported by the Natural Science Foundation of China (Grant no. 51002066).

References

1 K. Schmetzer, G. Schnorrer-Köhler and O. Medenbach, *Neues Jahrb. Mineral., Abh.*, 1985, **4**, 145–154.
2 X.-R. Qu and D.-C. Jia, *J. Cryst. Growth*, 2009, **311**, 1223–1228.
3 A. S. Shaporev, V. K. Ivanov, A. E. Baranchikov, O. S. Polezhaeva and Y. D. Tret'yakov, *Russ. J. Inorg. Chem.*, 2007, **52**, 1811–1816.
4 S. Mukhopadhyay, P. P. Das, S. Maity, P. Ghosh and P. S. Devi, *Appl. Catal., B*, 2015, **65**, 128–138.
5 N. Uekawa, S. Iahii, T. Kojima and K. Kakegawa, *Mater. Lett.*, 2007, **61**, 1729–1734.
6 M. Wang, Y. Zhang, Y. Zhou, F. Yang, E. J. Kim, S. H. Hahn and S. G. Seong, *CrystEngComm*, 2013, **15**, 754–763.
7 J. Wang, S. Hou, L. Zhang, J. Chen and L. Xiang, *CrystEngComm*, 2014, **16**, 7115–7123.
8 F. Demoisson, R. Piolet and F. Bernard, *Cryst. Growth Des.*, 2014, **14**, 5388–5396.
9 R. A. McBride, J. M. Kelly and D. E. McCormack, *J. Mater. Chem.*, 2003, **13**, 1196–1201.
10 P. Li, H. Liu, B. Lu and Y. Wei, *J. Phys. Chem. C*, 2010, **114**, 21132–21137.
11 M. Wang, Y. Zhou, Y. Zhang, S. H. Hahn and E. J. Kim, *CrystEngComm*, 2011, **13**, 6024–6026.
12 Y. Kozuka, A. Tsukazaki and M. Kawasaki, *Appl. Phys. Rev.*, 2014, **1**, 011303.
13 W. Kohn and L. J. Sham, *Phys. Rev.*, 1965, **140**, A1133.
14 J. P. Perdew, K. Burke and M. Ernzerhof, *Phys. Rev. Lett.*, 1996, **77**, 3865.
15 X. D. Liu, E. Y. Jiang, Z. Q. Li and Q. G. Song, *Appl. Phys. Lett.*, 2008, **92**, 252104.
16 T. Hitosugi, H. Kamisaka, K. Yamashita, H. Nogawa, Y. Furubayashi, S. Nakao, N. Yamada, A. Chikamatsu, H. Kumigashira, M. Oshima, Y. Hirose, T. Shimada and T. Hasegawa, *Appl. Phys. Express*, 2008, **1**, 111203.
17 O. Volnianska, P. Boguslawski, J. Kaczkowski, P. Jakubas, A. Jezierski and E. Kaminska, *Phys. Rev. B: Condens. Matter Mater. Phys.*, 2009, **80**, 245212.
18 R. M. Sheetz, I. Ponomareva, E. Richter, A. N. Andriotis and M. Menon, *Phys. Rev. B: Condens. Matter Mater. Phys.*, 2009, **80**, 195314.
19 X. Ma, B. Lu, D. Li, R. Shi, C. Pan and Y. Zhu, *J. Phys. Chem. C*, 2011, **115**, 4680–4687.
20 H.-C. Wu, Y.-C. Peng and C.-C. Chen, *Opt. Mater.*, 2013, **35**, 509–515.
21 S.-G. Park, B. Magyari-Köpe and Y. Nishi, *Phys. Rev. B: Condens. Matter Mater. Phys.*, 2010, **82**, 115109.
22 M. D. Segall, P. J. D. Lindan, M. J. Probert, C. J. Pickard, P. J. Hasnip, S. J. Clark and M. C. Payne, *J. Phys.: Condens. Matter*, 2002, **14**, 2717–2744.
23 C. Kilic and A. Zunger, *Phys. Rev. Lett.*, 2002, **88**, 095501.

24 H. D. Lutza, C. Jung, R. Mörtel, H. Jacobs and R. Stahl, *Spectrochim. Acta, Part A*, 1998, **54**, 893–901.
25 M. Y. Ghotbi, *J. Alloys Compd.*, 2010, **491**, 420–422.
26 M. Wang, E. J. Kim, J. S. Chung, E. W. Shin, S. H. Hahn, K. E. Lee and C. Park, *Phys. Status Solidi A*, 2006, **203**, 2418–2425.
27 X. L. Wu, G. G. Siu, C. L. Fu and H. C. Ong, *Appl. Phys. Lett.*, 2001, **78**, 2285–2287.
28 Y. Sun, G. M. Fuge, N. A. Fox, D. J. Riley and M. N. R. Ashfold, *Adv. Mater.*, 2005, **17**, 2477–2481.
29 S. Kundu, S. Sain, B. Satpati, S. R. Bhattacharyya and S. K. Pradhan, *RSC Adv.*, 2015, **5**, 23101–23113.
30 S. Sahoo, A. K. Arora and V. Sridharan, *J. Phys. Chem. C*, 2009, **113**, 16927–16933.
31 T. Premkumar, Y. S. Zhou, Y. F. Lu and K. Baskar, *ACS Appl. Mater. Interfaces*, 2010, **2**, 2863–2869.
32 G. H. Du, F. Xu, Z. Y. Yuan and G. van Tendeloo, *Appl. Phys. Lett.*, 2006, **88**, 243101.
33 E. de la Rosa, S. Sepúlveda-Guzman, B. Reeja-Jayan, A. Torres, P. Salas, N. Elizondo and M. J. Yacaman, *J. Phys. Chem. C*, 2007, **111**, 8489–8495.
34 T. Long, K. Takabatake, S. Yin and T. Sato, *J. Cryst. Growth*, 2009, **311**, 576–579.
35 D. Wu, Z. Bai and K. Jiang, *Mater. Lett.*, 2009, **63**, 1057–1060.
36 O. Mondal and M. Pal, *J. Mater. Chem.*, 2011, **21**, 18354–18358.
37 H. Zeng, G. Duan, Y. Li, S. Yang, X. Xu and W. Cai, *Adv. Funct. Mater.*, 2010, **20**, 561–572.
38 H. Usui, T. Sasaki and N. Koshizaki, *Appl. Phys. Lett.*, 2005, **87**, 063105.
39 G. Ballerini, K. Ogle and M.-G. Barthés-Labrousse, *Appl. Surf. Sci.*, 2007, **253**, 6860–6867.
40 J. M. Wu and Y.-R. Chen, *J. Phys. Chem. C*, 2011, **115**, 2235–2243.
41 S. Sepulveda-Guzman, B. Reeja-Jayan, E. de la Rosa, A. Torres-Castro, V. Gonzalez-Gonzalez and M. Jose-Yacaman, *Mater. Chem. Phys.*, 2009, **115**, 172–178.
42 S. Bai, L. Chen, S. Chen, R. Luo, D. Li, A. Chen and C. C. Liu, *Sens. Actuators, B*, 2014, **190**, 760–767.
43 Y. Y. Tay, T. T. Tan, F. Boey, M. H. Liang, J. Ye, Y. Zhao, T. Norby and S. Li, *Phys. Chem. Chem. Phys.*, 2010, **12**, 2373–2379.
44 I. Shalish, H. Temkin and V. Narayanamurti, *Phys. Rev. B: Condens. Matter Mater. Phys.*, 2004, **69**, 245401.